The topology of E/I recurrent networks regulates the effects of synaptic plasticity

Emmanouil Giannakakis, Oleg Vinogradov, Victor Buendía, Anna Levina
(Dated: July 11, 2023)

Synaptic plasticity is the primary mechanism for learning and memory in the brain. In recurrent neural networks, synaptic plasticity creates intricate feedback loops between population activity and connection strength. However, how the various topological features of brain networks, such as the diverse connectivity patterns of different neuron types, affect synaptic plasticity remains largely unknown. Here we investigate this question on the example of emergent excitatory and inhibitory co-tuning. This dynamical feature has been observed in cortical networks and was shown to be essential for efficient information processing. Computational models demonstrated that E/I co-tuning could arise from synaptic re-organization by a well-orchestrated plasticity protocol in low-noise feedforward networks. However, we show that the same plasticity protocol cannot give rise to E/I co-tuning in the presence of strong noise and unstructured recurrent connectivity. Using analytical methods and approximate Bayesian inference, we demonstrate that forming assembly structures in the recurrent connectivity can restore the ability of synaptic plasticity to produce E/I co-tuning, and we identify the optimal patterns for such co-tuning to emerge. In particular, we find that enhanced excitatory connectivity between similarly tuned neurons, combined with more homogeneous inhibitory connectivity, improves the ability of plasticity to produce co-tuning in an upstream population. Our results demonstrate how structured recurrent connectivity could control the ability of synaptic plasticity to adjust networks for efficient information processing.

I. INTRODUCTION

Synaptic plasticity is a fundamental mechanism of the nervous system, primarily associated with learning and memory formation [1]. Neural plasticity has been the subject of intense experimental investigation, which has revealed a large number of learning rules, secondary adaptive mechanisms, and homeostatic processes acting over multiple subsystems and neuron types [2] and following a wide range of timescales [3, 4].

Following these experimental findings, theoretical studies have ventured to model different plasticity mechanisms and identify the processes that underlie synaptic modification and its relationship to learning. Starting with early Hebbian models of synaptic plasticity in the 1940s, a large body of literature has accumulated focusing on more complex and biophysically plausible learning rules [5, 6], plasticity models for varied neuron types [7] and different homeostatic mechanisms [8]. Additionally, as both experimental understanding and simulation methods advance, there has been a more concerted effort towards identifying combinations of different plasticity mechanisms that can be associated with specific learning tasks such as assembly formation [9, 10] and novelty detection [11].

Input selectivity is a prevalent mechanism for encoding information in the nervous system [12]. Although originally observed in excitatory neurons, it was later it was established that inhibitory neurons also display input selectivity [13]. Furthermore, experimental studies have demonstrated that excitatory and inhibitory inputs (coming from similarly tuned E and I neurons) are highly correlated in cortical neurons (a given stimulus evokes near-simultaneous excitatory and inhibitory currents in a neuron that cancel out after some time) [14, 15]. This feature is called E/I *co-tuning*, and it was shown to optimize information transmission, for example, in the framework of efficient coding [16] or by enabling precise temporal computations [17]. The emergence of co-tuning is attributed to synaptic plasticity, and multiple theoretical studies have identified plasticity mechanisms leading to matching E/I selectivity in specific settings. These include studies focusing on how inhibitory plasticity rules can match static excitatory connectivity [7, 18, 19] and how various combinations of plasticity and diverse normalization mechanisms can enable the simultaneous development of coordinated excitatory and inhibitory connectivity in feedforward [20, 21] or recurrent settings [22–24].

So far, theoretical studies of plasticity have aimed at identifying the optimal parameters of individual learning rules and normalization mechanisms for specific tasks, such as the formation of input selectivity, in feed-forward or homogeneous recurrent networks. These simplified connectivities are very different from the highly non-trivial topologies of biological networks, which are known to display varied degrees of clustering and neuron type-specific connectivity patterns [25]. However, different network topologies are known to give rise to distinct neural dynamics; for example, clustering in recurrent network structure introduces correlations in the activity of similarly tuned neurons [26] that can fundamentally influence how synaptic plasticity shapes the connectivity of these networks. We hypothesize that there is a strong interdependence between the connectivity structure of recurrent networks and the ability of local plasticity mechanisms to perform specific learning tasks.

Here we investigate how the development of matching E/I input selectivity in an upstream neuron via synaptic plasticity can be influenced by the structure of recurrent connectivity in the input network. We combine excitatory and inhibitory plasticity rules [6, 7, 21] in a spiking network to develop detailed co-tuning of excitatory and inhibitory
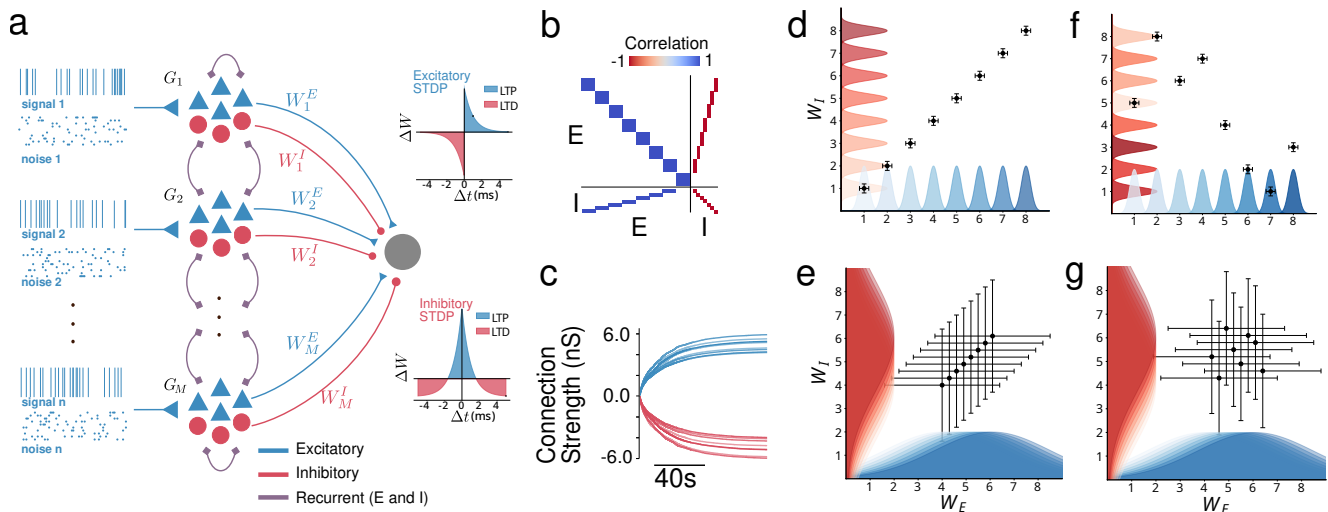
FIG. 1. **Emergence of co-tuning in a feedforward network a.** A diagram of the network. The purple recurrent connections are absent in the feedforward version of the model (panels b-f), but will be included in later sections. **b.** The modified (the sign of inhibitory activities is inverted) covariance matrix determines the convergence point of the plasticity protocol. Here we see a near-optimal matrix that leads to very clear co-tuning. **c.** The development of E and I weights in a feedforward network with very low noise leads to balanced and diverse feedforward connectivity. **d.** An illustration of feedforward connectivity that exhibits both balance and diversity. Different input groups are clearly distinct and the E and I weights for each group are correlated **e.** A balanced but not diverse connectivity. E/I co-tuning is maintained, but there is hardly any distinction between groups **f.** A diverse but not balanced connectivity. While each group is distinct from the others, there is no coordination of E and I connections from the same group **g.** In the absence of both balance and diversity the feedforward connectivity lacks any discernible pattern.

connectivity, and we demonstrate that the ability of these plasticity mechanisms to create co-tuning is significantly reduced in the presence of noise and random recurrent connectivity between the input neurons. We further show that the effects of recurrence and noise on E/I co-tuning can be fully ameliorated by the formation of synapse-type specific assemblies of neurons, characterized by local excitation and lateral inhibition, a well-observed pattern of cortical connectivity [27, 28]. Our findings demonstrate that network topology can significantly modulate the capacity of synaptic plasticity to generate input selectivity in upstream neurons by shaping the population activity of recurrent networks in lower areas. This highlights a synergistic interaction between structural connectivity and learning mechanisms that can enhance the computational capabilities of brain networks

II. RESULTS

A. Co-tuning and its self-organization by synaptic plasticity in a low-noise feedforward setting

We model a single postsynaptic read-out unit driven by a population of $N = 1000$ neurons. The pre-synaptic population is divided into M groups G_i, $i \in \{1, \ldots, M\}$. Each group is comprised of $n = N/M$ neurons, of which 80% are excitatory, and 20% are inhibitory. These neurons are driven by an identical, group-specific Poisson spike train — a shared external input. Additionally, each neuron receives low-intensity independent external noise [7]. This setting, depicted in Fig. 1a, leads to highly correlated firing among neurons of the same input group, which is a common setting for studying the effect of different plasticity rules [7, 20, 21].

Input selectivity develops when the post-synaptic neuron responds differently to inputs from different groups (by adjusting its firing rate). This happens when the excitatory feedforward projections are sufficiently diverse between pre-synaptic groups, which leads to groups with stronger feedforward connections eliciting stronger post-synaptic responses upon activation. Moreover, connections from neurons with highly correlated firing (i.e., from the same group) should have a similar strength. To quantify this feature of the network, we define a diversity metric,

$$D = 1 - \frac{1}{M \cdot \mathrm{Std}\left(W^E\right)} \sum_{i=1}^{M} \mathrm{Std}(W_{G_i}^E), \tag{1}$$
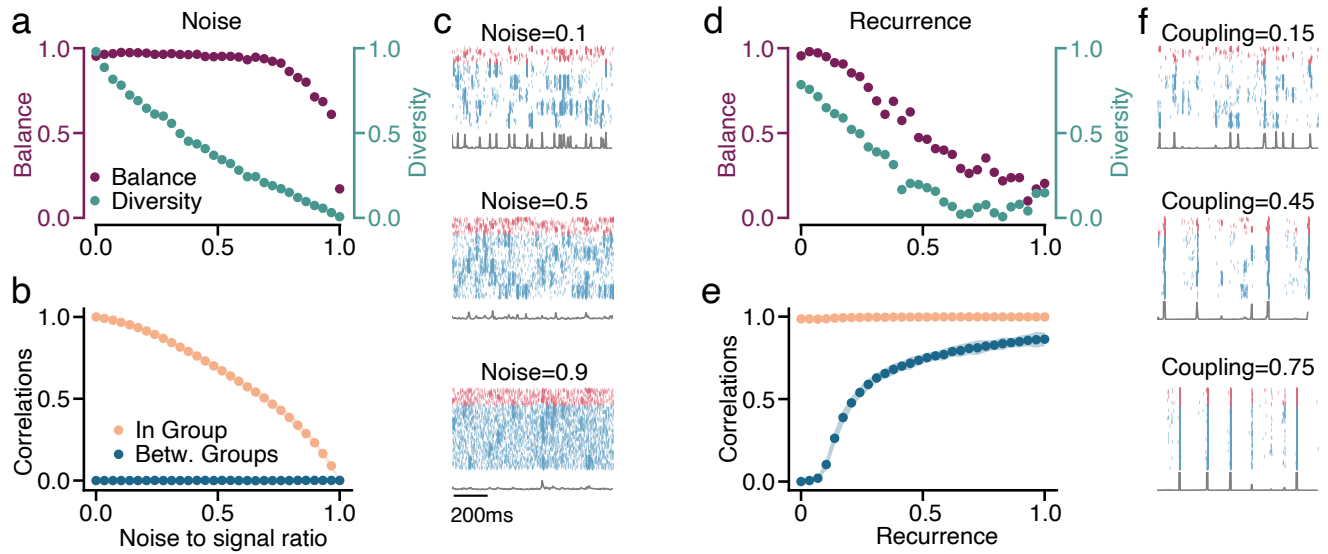
FIG. 2. **Noise and Recurrence Destroy E/I Co-Tuning. a.** An increase in the input noise leads to a reduction in diversity (green) and, for larger noise intensities, also balance (purple). **b.** The increase in noise leads to a the decrease in in-group correlation, while the between-group correlation remains low. **c.** As the noise increases (noise level is indicated above each panel), the spiking activity becomes more asynchronous. **d.** An increase in the recurrent coupling strength leads to a rapid decrease in balance and diversity, which is caused by (**e.**) an increase in the between-group correlation. **f.** The spiking activity becomes more synchronous as the coupling strength increases.

where $W^E \in \mathbb{R}^{n \times n}$ is the set of excitatory feedforward connection weights and $W^E_{G_i}, \in \mathbb{R}^{n \times n}$ is the subset of excitatory feedforward connection weights from input group i and $\mathrm{Std}(\cdot)$ denotes the standard deviation. Diversity $D \in [0, 1]$ equals unity when the feedforward connections are similar within a group but different across groups; D is close to zero when pre-synaptic neurons are randomly projecting to the post-synaptic neuron.

Brain networks are characterized by a balance of excitatory and inhibitory currents [15, 29, 30]. For a neuron to be balanced, the average inhibitory current must be equal to the average excitatory current during a (relatively short) time window. In our setting, we aim to achieve a detailed balance, where the E and I currents match over very small time windows. This type of balance has been linked to efficient coding [16, 31] and the ability to process multiple signals [32] and can be achieved if the excitatory and inhibitory connection strengths of each input group are matching. This setting results in the near-total canceling out of E and I currents following a small delay generated by the difference in the synaptic timescales [7, 32].

To quantify detailed balance, we use the Pearson correlation coefficient between the mean excitatory and inhibitory weights of each group,

$$B = \frac{\mathrm{Cov}\left(\langle W^E_G \rangle, \langle W^I_G \rangle\right)}{\mathrm{Std}\left(\langle W^E_G \rangle\right) \cdot \mathrm{Std}\left(\langle W^I_G \rangle\right)}, \tag{2}$$

where $\langle W^k_G \rangle = \left(\langle W^k_{G_1} \rangle, \langle W^k_{G_2} \rangle, \ldots, \langle W^k_{G_m} \rangle\right)$, $k \in \{I, E\}$ and $\langle W^k_{G_i} \rangle$ is the average projection weight from the excitatory $(k = E)$ or inhibitory $(k = I)$ neurons in group i, and $\mathrm{Cov}(x_1, x_2)$ denotes the covariance of the variables x_1 and x_2. In networks with high detailed balance B, the strength of incoming E and I currents is highly correlated.

We verify that high diversity $(D \approx 1)$ and detailed balance $(B \approx 1)$ can organically emerge via a combination of plasticity mechanisms in the feedforward connections. Specifically, the excitatory connections follow the triplet Hebbian STDP rule [33] and the inhibitory connections follow a homeostatic Hebbian rule [7]. We additionally use competitive normalization in both the inhibitory and excitatory connections which amplifies small transient differences between the firing rates of different input groups and leads to the development of input selectivity [21]. The plasticity protocol consistently generates near-perfect E-I balance and creates strong input selectivity, Fig. 1c.

The point at which the feedforward weights converge is fully determined by the covariance matrix of the presynaptic neurons' activities. Specifically, it has been demonstrated [7, 20, 21] that the fixed points of the weight dynamics are eigenvectors of the modified covariance matrix:

$$\overline{C} = \left\langle \begin{pmatrix} EE^T & -IE^T \\ EI^T & -II^T \end{pmatrix} \right\rangle \tag{3}$$
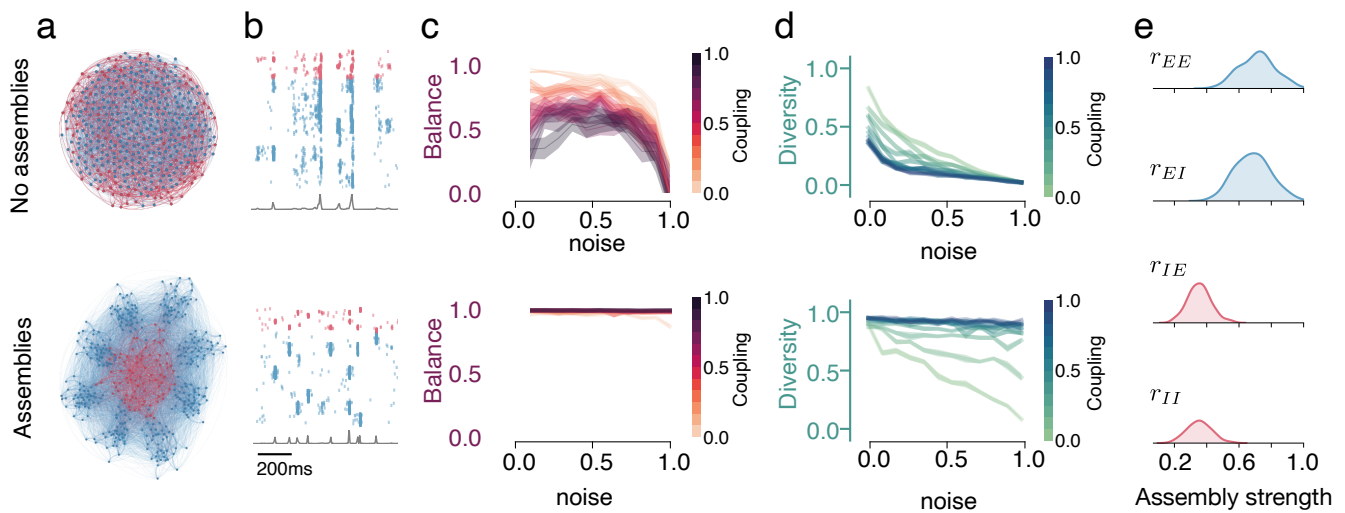
FIG. 3. **Optimized assemblies of neurons restore the co-tuning in recurrent noisy networks.** Top row — networks with uniform connectivity, bottom — networks with inferred optimal assembly strengths. **a.** Diagram of the network, with uniform connectivity and inferred optimal assembly strengths. **b.** Examples of stimulus-driven activity of a homogeneous (top) and with optimized assemblies (bottom) population. **c.** Balance in homogeneous (top) and optimized assemblies (bottom) networks with different strengths of noise and coupling. **d.** Same for diversity. Assemblies restore co-tuning even with strong noise if given sufficient coupling strength, but for homogeneous networks, the strong coupling is detrimental to the development of co-tuning. **e.** Approximate posterior distributions of optimal excitatory and inhibitory assemblies strength.

where $E \in \mathbb{R}^n$ and $I \in \mathbb{R}^n$ are the firing rates of the presynaptic excitatory and inhibitory neurons, respectively, and $\langle \cdot \rangle$ stands for the average over time, Fig. 1b. We verify that in our model, the feedforward weights indeed converge to an eigenvector of the covariance matrix (see Supplementary 2).

B. Noise and recurrent connectivity compromise the ability of STDP to produce E/I co-tuning

Strictly feed-forward and low-noise circuits are unrealistic approximations whose dynamics might deviate significantly from the dynamics observed in real brain networks. Thus, we introduce noise and recurrent connectivity in our network, both ubiquitously present in biological networks [34, 35]. First, we investigate how they individually affect the emerging E/I co-tuning by changing the structure of the activity covariance matrix. Then we examine ways in which different connectivity structures can ameliorate these effects.

As the ratio of noise to signal increases, the cross-correlations within each input group decrease, while the cross-correlations between neurons of different input groups remain very low, Fig. 2b. We control the noise level by changing the ratio of signal to noise spikes. Signal spikes are received by all neurons of the same group, while noise spikes come from the neuron-specific Poisson process independently for each neuron. This allows us to vary the signal-to-noise ratio while keeping the number of incoming spikes the same. The effect of this in-group decorrelation is an increased variability in the learned projections to the postsynaptic neuron from neurons of the same input group and, thus, a decrease in the resulting diversity. At the same time, increased noise has only a small effect on the correlation between E and I populations as measured by the balance metric, which visibly declines only once the noise becomes overwhelmingly stronger than the input (more than 80% incoming spikes are not shared between neurons of the same group), Fig. 2a.

Recurrent connectivity in the pre-synaptic network introduces cross-correlations between the neurons from different input groups, which compromises both diversity and balance. To test the extent of this effect, we connect the N presynaptic neurons (creating a recurrent network) with connection probability p, and use the coupling strength W as a control parameter. Initially, we only consider fully-connected networks ($p = 1$). By changing W, we can control the ratio between the input received from the feedforward connections (whose rate and connection strength is fixed) and the other neurons in the network via recurrent connectivity. The recurrent connectivity increases cross-correlations between groups while maintaining the high correlation within each input group, Fig. 2e. The effect of these cross-correlations is stronger than the effect of the noise since they affect both the diversity and the E/I balance, both of which decline as the recurrent connections become stronger Fig. 2d.

The combination of noise and recurrent connectivity affects both in-group and between-group correlations, resulting
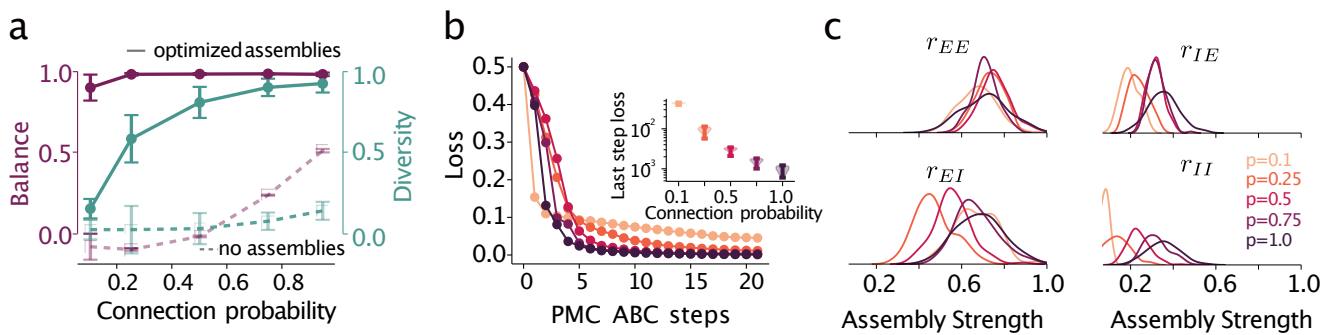
FIG. 4. Assemblies improve co-tuning and allow for co-tuning in sparse networks. **a.** E/I balance (purple) and weights diversity (teal) in the networks with assemblies compared to non-structured networks (dashed lines), error bars — standard deviation. The noise level is 0.1 for all sparsities, and the coupling is 0.85 (scaled by $1/p$). **b.** Loss for the sparser networks is higher, which results in the overall worse performance; inset shows the loss for 50 accepted samples at the last ABC step. **c.** Posterior distributions of all assembly strengths change with sparsity. Sparser networks require weaker inhibitory assemblies (more uniform connections) to produce co-tuning.

in a reduction of balance and diversity as the noise and recurrent connection strength increase, Fig. 3c-d (top).

We develop a formal description of the effect of noise and recurrence on the covariance structure in a simplified linear neural mass model. To this end, we consider $M = 8$ mesoscopic units instead of the previously studied M inter-connected groups, represented by continuous rate variables $x_j(t)$, $j = 1, \ldots, M$. These units evolve in time, subject to stochastic white noise. The linear approximation is justified for any system at a stationary state with a constant average firing rate, and it serves as a simplified model for a wide range of parameters of the spiking network (for details on the linear model and its relation to the spiking network, (see Supplementary 4).

In this simplified case, it is possible to derive analytical equations for all the relevant in- and between-group covariances, which yield the correlation coefficients. These covariances are the solution to a linear system of equations, which can be obtained exactly using numerical methods. Furthermore, one can find close-form solutions in some simple scenarios. For example, in the case of a completely homogeneous network, where all coupling weights are the same, correlation coefficients can be written explicitly (see Supplementary 4). If the coupling strength increases $W \to +\infty$, all correlations grow to 1 as $1 - \mathcal{O}(1/W^2)$, while they decrease to $MW/(M-1)^2 + \mathcal{O}(r^{-2})$ when increasing the noise to signal ratio $r \to 0_+$. Both cases eliminate any possible differentiation between the groups, thus compromising the ability of the plasticity mechanisms to create diversity D. Another observation is that in the linear network, increasing noise affects the correlation coefficient quadratically, while coupling increases it linearly. Therefore, since $r < 1$, increasing the coupling has a larger impact on the co-tuning, a consequence that is recovered in the spiking network, Fig. 2.

C. Neuronal type-specific assemblies restore the ability of STDP to produce co-tuning

The homogeneous all-to-all connectivity that we have examined so far is not a realistic assumption and could be particularly detrimental to the self-organization of co-tuning. Thus, we examine the impact of different types of inhomogeneous connectivity. In particular, using the idea of functional assemblies (strongly connected neurons that are tuned to the same stimulus), we study whether stronger recurrent connectivity between neurons of the same input group can lead to beneficial correlations in the population activity.

We aim to maintain the total recurrent input a neuron receives constant (the fraction of input coming from the signal/noise vs the other neurons in the recurrent network) while using the ratio of input coming from neurons of the same vs other input groups as a control parameter. Since we want to vary this ratio independently for each connection type, we define a metric of assembly strength as:

$$r_{ab} = \frac{C_{\text{in}}^{ab}}{C_{\text{in}}^{ab} + C_{\text{out}}^{ab}} = \frac{W_{\text{in}}^{ab}}{W_{\text{in}}^{ab} + (M-1) \cdot W_{\text{out}}^{ab}}, \quad a, b \in \{E, I\}, \tag{4}$$

where C_{in}^{ab} in the total input a neuron of type b receives from neurons of type a, for $a, b \in \{E, I\}$, of its own input group and C_{out}^{ab} is the total input a neuron of type b receives from neurons of type a, for $a, b \in \{E, I\}$, from all other

input groups, W_{in}^{ab} the connection strength between neurons of the same group and W_{out}^{ab} the connection strength between neurons of different groups.

We vary assembly strengths for each type of connection r_{EE}, r_{EI}, r_{IE}, and r_{II} while keeping the total input to a neuron $C_{\text{in}}^{ab} + C_{\text{out}}^{ab} = \frac{p \cdot N}{M} \cdot (W_{\text{in}}^{ab} + (M-1) \cdot W_{\text{out}}^{ab}) =: p \cdot N \cdot W$ constant. Here W is the average coupling strength, and p is the recurrent connection probability. As in the network without assemblies, for now, we consider fully connected networks ($p = 1$). Thus, we can vary the fraction of input coming to a neuron from its own input group without changing the total recurrent E or I input it receives.

In the reduced linear neural mass model, we compute analytically the optimal assembly strengths (Supplementary 4) and find that strong local excitation and dispersed inhibition restore the desired covariance structure in the network's activity. We find that for all combinations of noise and sufficiently strong recurrent connectivity, strong excitatory assemblies (high r_{EE} and r_{EI}) and uniform inhibitory connectivity (low r_{IE} and r_{II}) allow the correlating excitatory currents to remain mostly within the input group/assembly and maintain high in-group correlation, while the diffused inhibitory currents reduce correlations between groups. Still, since the reduced model does not account for many essential features of the spiking network, like sparsity of connections, in-group interactions between neurons of the same type, and non-stationary dynamical states of the groups, the analytic solution obtained for the linear neural mass model can serve to develop intuition, but the results need to be validated for the recurrent spiking network.

To capture the effect of various assembly strengths on balance and diversity in the spiking network, we can use as a proxy their impact on the covariance structure of the spiking network's activity. Thus, we search for combinations of assembly strength $r_{EE}, r_{EI}, r_{IE}, r_{II}$ that lead to the covariance structure that is associated with detailed E/I balance ($B \approx 1$) and maximum weight diversity ($D \approx 1$). To this end, we use sequential Approximate Bayesian Computation (ABC) [36] to minimize a loss function defined to be zero when the in-group correlations are equal one and all between-group correlations vanish (for details, see Methods). This method allows us to find the approximate posterior distribution of network parameters (assembly strengths) that minimize the loss. Afterward, we verify whether connectivity parameters sampled from the approximate posterior lead to the emergence of co-tuning in the post-synaptic neuron.

Networks with optimized assemblies largely regain the ability to develop E/I co-tuning despite the presence of noise and recurrent connectivity. Assembly strengths that are drawn from the approximate posterior result in a covariance structure very similar to the one observed in a feedforward/low noise network, which allows the plasticity to produce a near-optimal structure in the feedforward connections, Fig. 3c-d (bottom). We find that the optimal assembly structure involves very strong $E \to E$ and $E \to I$ assemblies and medium-strength $I \to E$ and $I \to I$, Fig. 3e.

This connectivity pattern is similar to the optimal pattern of the reduced linear model, albeit with the difference that the reduced model predicted optimal performance for uniform inhibitory weights (i.e., no inhibitory assemblies, $r_{IE} = r_{II} = 0$). This difference can be attributed to the more complex dynamics of the spiking network that require some degree of local inhibition to prevent extreme bursting behaviors (see Supplementary 3).

D.   The sparsity of a network's recurrent connectivity shifts the optimal assembly structure

Biological neural networks are usually very sparsely connected [37–39] and the sparsity of connections is associated with distinct dynamics [40]. We observed that the impact of noise and recurrence on the deterioration of balance and weight diversity in sparse networks without assemblies is qualitatively similar to fully-connected networks. Thus, we examined the ability of neuronal assemblies to produce activity that restores balance and weight diversity in sparsely connected recurrent networks that receive noisy input.

The optimal assembly strength values depend on sparsity levels. We use ABC to discover the approximate posterior distribution of assembly strengths for 5 different levels of sparsity, corresponding to the probability of connection $p = 1.0$, $p = 0.75$, $p = 0.5$, $p = 0.25$, and $p = 0.1$. We preserve the total input per neuron across different sparsities by scaling the coupling strength inversely proportional to p. The optimal strength of most assemblies is reduced as the connection probability is decreased, Fig. 4c. Specifically, we find that all but $E \to E$ assemblies should be weaker in sparser networks, with the greatest decrease observed in the $I \to I$ assemblies that completely disappear for very sparse networks.

As sparsity increases, the ability of assemblies to improve the tuning diminishes. After 21 ABC steps, the overall loss is larger for the sparse networks than for fully-connected networks and increases with sparseness, Fig. 4b. Therefore, despite an improvement in the tuning metrics for most sparse networks (compare the dashed and solid lines in Fig. 4a), particularly diversity is strongly affected by sparseness and cannot be recovered by assemblies to the same extent as for the fully connected networks, Fig. 4a. This reduced effectiveness is expected, given the smaller number of connections and the greater variance in the network's connectivity.

III.   DISCUSSION

Synaptic plasticity is theorized to be responsible for the formation of input selectivity across brain hierarchies, including in brain areas that only receive input from highly recurrent networks. Here, we demonstrated how the topology of the recurrent connectivity could hinder or boost the ability of synaptic plasticity mechanisms [7, 18, 20, 21] to generate input selectivity in neurons of higher areas. We find that strong excitatory connectivity among neurons tuned to the same input, combined with broader inhibition, creates population activity that enables the formation of input selectivity by plasticity.

How different plasticity mechanisms shape neural connectivity, such as the formation of E/I co-tuning [7, 18, 20, 21] in feedforward networks or of neural assemblies in recurrent networks [7, 10, 41], have been a topic of extensive theoretical research. Nevertheless, the opposite effect - the ways in which connectivity can shape the effects of synaptic plasticity - has only been studied in very specialized cases[42]. This omission has partially obscured the two-way interaction between connectivity and synaptic plasticity in biological neural networks. While synaptic plasticity constantly modifies some aspects of neural connectivity, it acts within the many constraints of network topology that are either constant throughout an organism's lifetime or change via structural adaptation mechanisms that act on timescales slower than synaptic plasticity [43, 44]. Effectively, this means that synaptic plasticity modifies the details of highly intricate network structures that result in neuronal activity very different from those of random networks [9, 45]. Given that most synaptic plasticity mechanisms fundamentally depend on the statistics of network activity, it is reasonable to assume that the behavior of synaptic plasticity is highly constrained by the network topology.

Cortical networks are known to be highly clustered [46], and the clustering has functional as well as spatial determinants. For example, neurons that share common inputs [47] or targets [48] are more likely to form recurrent connections between themselves [49]. Clustered networks are known to display distinct dynamics characterized by slower timescales that can be useful for computations [26, 50]. Additionally, there is strong evidence that groups of highly interconnected neurons (neuronal assemblies) share common functions within recurrent networks [24, 51, 52]. Moreover, evidence has accumulated [53, 54] that different neuron types (excitatory and inhibitory subtypes) follow distinct spatial connectivity patterns, which have implications for neural computation [55]. Thus, our findings complement the ongoing research on recurrent neural connectivity in biological networks and their computational implications by suggesting a link between specific connectivity patterns and local learning via synaptic plasticity.

While the connectivity pattern we identify in our study is biologically plausible, the extent to which it is realized *in vivo* remains unclear. Further experimental studies in the connectivity patterns of different neuron types are necessary to be able to effectively model different network topologies and study their dynamics. Future studies could uncover the mechanisms by which the synapse-type specific assembly structures we identify can emerge and be maintained in plastic networks. Potential mechanisms include structural plasticity and variation in the learning rates of different synaptic types. Additionally, the presence of different regulatory interneurons, which has been linked with assembly formation [56], could play a role in modulating the relative assembly strengths of different connections.

For the purposes of our study, we parameterized the network topology by adopting a quantitative metric for the strength of different types of neuronal assemblies. This resulted in a low-dimensional parameter space and allowed us to use rejection sampling-based ABC [36] to infer the optimal assembly strengths. One limitation of this technique is that it suffers from the curse of dimensionality and typically requires a large simulation budget [57, 58]. Therefore, extensions of the current work using higher dimensional connectivity parameters or simultaneous inference of the connectivity and neuron parameters will require more efficient simulation-based methods such as neural posterior estimation [59]. Alternatively, direct optimization of each individual recurrent weight via gradient-based methods [60, 61] may uncover more intricate topological patterns that are not limited to the specific network parametrization we chose.

To summarize, we identified how particular connectivity structures could be a favorable or detrimental substrate for plasticity to develop co-tuning of excitation and inhibition. Our study is a first step in illuminating the two-way dependence between the topological features of a network and synaptic plasticity that can motivate further research on this intricate interaction.

IV.   MATERIALS AND METHODS

Neuron Model

We modelled all neurons of our networks as leaky integrate-and-fire (LIF) neurons with leaky synapses. The evolution of their membrane potential is given by the ODE

$$C_m \cdot \frac{dV(t)}{dt} = g_{\text{leak}} \cdot (V_{\text{rest}} - V(t)) + g_I(t) \cdot (V_I - V(t)) - g_E(t) \cdot (V_E - V(t)), \tag{5}$$

where V_{rest} is the neuron's resting potential, V_E, V_I are the excitatory and inhibitory reversal potentials and g_{leak} the leak conductance. Additionally, the excitatory and inhibitory conductances g_E, g_I decay exponentially over time and get boosts upon excitatory or inhibitory pre-synaptic spiking, respectively, as

$$\tau_E \cdot \frac{dg_E(t)}{dt} = -g_E(t) + \overline{g_E} \cdot \sum_j W_j^E \cdot \sum_f \delta(t - t_j^f),$$

$$\tau_I \cdot \frac{dg_I(t)}{dt} = -g_I(t) + \overline{g_I} \cdot \sum_j W_j^I \cdot \sum_f \delta(t - t_j^f). \tag{6}$$

Here t_j^f denotes the time at which the f-th spike of the $j-$th neuron happened. When the membrane potential reaches the spiking threshold V_{th}, a spike is emitted, and the potential is changed to a reset potential V_{reset}.

Network Input

The external input to each of the 1000 pre-synaptic neurons is the mixture of two Poisson spike trains. The first Poisson spike train is shared with all the other neurons of the same group, while the second Poisson spike train is the individual noise of the neuron,

$$C_{\text{total}} = C_{\text{signal}} + C_{\text{noise}}, \tag{7}$$

where $C_{\text{signal}} \sim \text{Poisson}((1-c) \cdot r)$ and $C_{\text{noise}} \sim \text{Poisson}(c \cdot r)$. Here, r is the total firing rate of the input, and c is the strength of the noise. C_{signal} is the same for all neurons of the same input group, while C_{noise} is individual to each neuron

Plasticity

Triplet excitatory STDP

The feedforward excitatory connections are modified according to a simplified form of the triplet STDP rule [6], which has been shown to generalize the Bienenstock–Cooper–Munro (BCM) rule [5] for higher-order correlations [33]. The firing rates of the pre-synaptic excitatory neurons and the post-synaptic neuron are approximated by traces with two different timescales,

$$\tau_1^{estdp} \cdot \frac{dy_k^E}{dt} = -y_k^E + \sum_f \delta(t - t_k^f), \tag{8a}$$

$$\tau_2^{estdp} \cdot \frac{dz_k^E}{dt} = -z_k^E + \sum_f \delta(t - t_k^f), \tag{8b}$$

$$\tau_1^{estdp} \cdot \frac{dx_1}{dt} = -x_1 + \sum_f \delta(t - t_x^f), \tag{8c}$$

$$\tau_2^{estdp} \cdot \frac{dx_2}{dt} = -x_2 + \sum_f \delta(t - t_x^f), \tag{8d}$$

where $\tau_1^{estdp} < \tau_2^{estdp}$ are the two timescales of the plasticity rule, y_k^E, z_k^E and x_1, x_2 represent the slow and fast traces of the k-th excitatory pre-synaptic and the single post-synaptic neuron respectively while t_k^f and t_x^f are their respective firing times. The connection weights are updated upon pre and post-synaptic spiking according to

$$\Delta W_k^E = \eta_E \cdot A_{LTP} \cdot x_1 \cdot z_k^E \cdot \sum_f \delta(t - t_k^f) - \eta_E \cdot A_{LTD} \cdot x_2 \cdot y_k^E \cdot \sum_f \delta(t - t_x^f), \tag{9}$$

where η_E is the excitatory learning rate and A_{LTP}, A_{LTD} the amplitudes of long term depression and potentiation respectively.

Inhibitory STDP

We used the homeostatic STDP rule first proposed in [7] for the inhibitory feedforward connections. Approximations of the firing rates are kept via a trace for each of the pre-synaptic inhibitory neurons as well as the post-synaptic neuron,

$$\tau^{istdp} \cdot \frac{dy_k^I}{dt} = -y_k^I + \sum_f \delta(t - t_k^f), \tag{10a}$$

$$\tau^{istdp} \cdot \frac{dx}{dt} = -x + \sum_f \delta(t - t_x^f), \tag{10b}$$

where τ^{istdp} is the single timesclae of the plasticity rule, y_k^I and x are the traces of the the k_{th} inhibitory pre-synaptic and the single post-synaptic neuron, and t_k^f, t_x^f are their respective spike times. The connection weights are updated upon pre and post-synaptic spiking as

$$\Delta W_k^I = \eta_I \cdot (x - 2\rho_0 \tau^{stdp}) \cdot \sum_f \delta(t - t_k^f) + \eta_I \cdot y_k^I \cdot \sum_f \delta(t - t_x^f). \tag{11}$$

Here, η_I is the inhibitory learning rate, and ρ_0 is the target rate of the post-synaptic neuron.

Synaptic Scaling

Due to the instability of the triplet STDP rule, some sort of normalization mechanism is necessary to constrain weight development. We use the novel competitive normalization protocol first proposed in [21], which we adapt for spiking neurons. The normalization is separately applied to both excitatory and inhibitory incoming connections,

$$W_k^A \leftarrow W_k^A \left(1 - \eta_N + \eta_N \cdot \frac{W_{target}^A}{\sum_{i=1}^{N_A} W_i^A}\right), \quad A \in \{E, I\}. \tag{12}$$

Where W_{target}^A is the target total weight of each connection type and η_N is the normalization learning rate. The normalization maintains the sum of the excitatory and the sum of the inhibitory feedforward connections weights close to the set target total weights W_{target}^E and W_{target}^I.

Approximating the posterior distribution of the model parameters

To estimate the set of parameters that lead to high in-group correlations and low out-group correlations, we used simulation-based inference [57]. The basic idea is to use simulation with known parameters to approximate the full posterior distributions for the model given the required output, i.e., the distribution of parameters and samples from which produce the required correlation structure. To approximate the posterior distribution we use sequential Approximate Bayesian Computation (ABC) [36]. We define a loss function that maximizes in-group correlations and minimizes between-group correlations:

$$\mathcal{L} = -\alpha C_{in}^2 - \beta \left[(1 - C_{out}^{EE})^2 + (1 - C_{out}^{EI})^2 + (1 - C_{out}^{II})^2\right] \tag{13}$$

We define a uniform prior $p(\theta)$. A set of parameters $\theta = [r_{ee}, r_{ei}, r_{ie}, r_{ii}]$ is sampled from it and used to run the simulations for 3 seconds. From the simulation results, correlations are computed, which allows us to obtain the loss. We accept a parameter set if the loss is below the error ϵ, and keep sampling until the number of accepted samples is 60. We use the kernel density estimate on the accepted samples to obtain an approximate posterior. Next, we rescale this approximate posterior with the original prior to obtain a proposal distribution that we use as a prior in the next step of the ABC. In each step, we reduce ϵ by setting it to the 75th percentile of the losses for the accepted samples (see [36] for more details). As a rule, we run 20 to 30 steps of the sequential ABC until the loss converges. We run separate fits for networks with different levels of sparsity with connection probabilities $p = 0.1, 0.25, 0.5, 0.75, 1.0$. The fitting was done using a modified version of the simple-abc toolbox https://github.com/rcmorehead/simpleabc/ for python.

Reduced model

The dynamics of the system can be studied analytically using a simplified, reduced linear model. Here, each pair of variables (x_i, y_i) represents the excitatory and inhibitory mean firing rate of a neuron group. In theory, these variables display complicated non-linear interactions that arise from the microscopic details of the LIF spiking network and synapse dynamics. However, in the stationary state –and away from any critical point– a linearised model can capture the essential features of the correlations between different populations.

Internal noise, modelled as independent Poisson trains to each individual neuron, becomes Gaussian white noise in the large-population limit, characterized by zero mean and variance σ_{int}. Each population is affected by different internal fluctuations. For simplicity, external noise, which is applied as the same train of Poisson spikes to all the neurons inside an input group, will also be approximated as a Gaussian white noise of mean η_0 and variance σ_{ext}.

Therefore, the simplified linear model reads

$$\dot{x}_i = ax_i + by_i + \frac{1}{M-1}\sum_{j\neq i}\left(W^{EE}x_j + W^{EI}y_j\right) + \sigma_{\text{int}}\xi_i^x(t) + \sigma_{\text{ext}}\eta_i(t) + \eta_0, \tag{14a}$$

$$\dot{y}_i = cx_i + dy_i + \frac{1}{M-1}\sum_{j\neq i}\left(W^{IE}x_j + W^{II}y_j\right) + \sigma_{\text{int}}\xi_i^y(t) + \sigma_{\text{ext}}\eta_i(t) + \eta_0, \tag{14b}$$

where M is the number of populations, a, b, c, d are parameters controlling in-group recurrent coupling, and W^{EE}, W^{EI}, W^{IE}, W^{II} are couplings between different clusters. Internal noise for each population is represented by $\xi_i^{x,y}(t)$, while external noise is notated as $\eta_i(t)$. All noises are uncorrelated, meaning that

$$\left\langle \xi_i^c \xi_j^{c'} \right\rangle = \delta_{cc'}\delta_{ij}\delta(t-t'), \tag{15a}$$

$$\langle \xi_i^c(t)\eta_j(t')\rangle = 0 \quad \forall i,j,t,t', \tag{15b}$$

$$\langle \eta_i(t)\eta_j(t')\rangle = \delta_{ij}\delta(t-t'), \tag{15c}$$

with $c, c' = \{x, y\}$, and where $\langle \ldots \rangle$ represents an ensemble average, i.e., an average over noise realizations. From this model, it is possible to obtain closed equations for Pearson correlation coefficients (see Supplementary 4 for details). Notice that stochastic differential equations are never complete without an interpretation, and we choose to interpret these in the Itô sense, which will be relevant for computations.

V.   ACKNOWLEDGEMENTS

[1] A. Citri and R. Malenka, Synaptic plasticity: Multiple forms, functions, and mechanisms, Neuropsychopharmacology : official publication of the American College of Neuropsychopharmacology **33**, 18 (2008).

[2] R. S. Larsen and P. J. Sjöström, Synapse-type-specific plasticity in local circuits, Current Opinion in Neurobiology **35**, 127 (2015), circuit plasticity and memory.

[3] G. G. Turrigiano, The self-tuning neuron: Synaptic scaling of excitatory synapses, Cell **135**, 422 (2008).

[4] A. Watt and N. Desai, Homeostatic plasticity and stdp: keeping a neuron's cool in a fluctuating world, Frontiers in Synaptic Neuroscience **2**, 10.3389/fnsyn.2010.00005 (2010).

[5] E. Bienenstock, L. Cooper, and P. Munro, Theory for the development of neuron selectivity: orientation specificity and binocular interaction in visual cortex, Journal of Neuroscience **2**, 32 (1982), https://www.jneurosci.org/content/2/1/32.full.pdf.

[6] J.-P. Pfister and W. Gerstner, Triplets of spikes in a model of spike timing-dependent plasticity, Journal of Neuroscience **26**, 9673 (2006), https://www.jneurosci.org/content/26/38/9673.full.pdf.

[7] T. P. Vogels, H. Sprekeler, F. Zenke, C. Clopath, and W. Gerstner, Inhibitory plasticity balances excitation and inhibition in sensory pathways and memory networks, Science **334**, 1569 (2011), https://science.sciencemag.org/content/334/6062/1569.full.pdf.

[8] T. Elliott and N. R. Shadbolt, Multiplicative synaptic normalization and a nonlinear hebb rule underlie a neurotrophic model of competitive synaptic plasticity, Neural Comput. **14**, 1311–1322 (2002).

[9] A. Litwin-Kumar and B. Doiron, Formation and maintenance of neuronal assemblies through synaptic plasticity, Nature communications **5**, 5319 (2014).

[10] O. Mackwood, L. B. Naumann, and H. Sprekeler, Learning excitatory-inhibitory neuronal assemblies in recurrent networks, eLife **10**, e59715 (2021).

[11] A. Schulz, C. Miehl, I. Berry, Michael J, and J. Gjorgjieva, The generation of cortical novelty responses through inhibitory plasticity, eLife **10**, e65309 (2021).

[12] M. Riesenhuber and T. Poggio, Hierarchical models of object recognition in cortex, Nature neuroscience **2**, 1019 (1999).

[13] A. M. Kerlin, M. L. Andermann, V. K. Berezovskii, and R. C. Reid, Broadly tuned response properties of diverse inhibitory neuron subtypes in mouse visual cortex, Neuron **67**, 858 (2010).

[14] J. Isaacson and M. Scanziani, How Inhibition Shapes Cortical Activity, Neuron **72**, 231 (2011).

[15] M. Okun and I. Lampl, Instantaneous correlation of excitation and inhibition during ongoing and sensory-evoked activities, Nature Neuroscience **11**, 535 (2008).

[16] S. Deneve and C. Machens, Efficient codes and balanced networks, Nature Neuroscience **19**, 375 (2016).

[17] A. Bhatia, S. Moza, and U. S. Bhalla, Precise excitation-inhibition balance controls gain and timing in the hippocampus, eLife **8**, e43415 (2019).

[18] Y. Luz and M. Shamir, Balancing feed-forward excitation and inhibition via hebbian inhibitory synaptic plasticity, PLOS Computational Biology **8**, 1 (2012).

[19] S. Khajehabdollahi, E. Giannakakis, J. Prosi, and A. Levina, Reservoir computing with self-organizing neural oscillators, The 2021 Conference on Artificial Life Proceedings 10.1162/isal_a_00409 (2021), 78, https://direct.mit.edu/isal/proceedings-pdf/isal/33/78/1929805/isal_a_00409.pdf.

[20] C. Clopath, T. P. Vogels, R. C. Froemke, and H. Sprekeler, Receptive field formation by interacting excitatory and inhibitory synaptic plasticity, bioRxiv 10.1101/066589 (2016), https://www.biorxiv.org/content/early/2016/07/29/066589.full.pdf.

[21] S. Eckmann and J. Gjorgjieva, Synapse-type-specific competitive hebbian learning forms functional recurrent networks, bioRxiv 10.1101/2022.03.11.483899 (2022), https://www.biorxiv.org/content/early/2022/03/14/2022.03.11.483899.full.pdf.

[22] F. Effenberger, J. Jost, and A. Levina, Self-organization in balanced state networks by stdp and homeostatic plasticity, PLoS computational biology **11**, e1004420 (2015).

[23] R. Larisch, L. Gönner, M. Teichmann, and F. H. Hamker, Sensory coding and contrast invariance emerge from the control of plastic inhibition over emergent selectivity, PLOS Computational Biology **17**, 1 (2021).

[24] C. Miehl and J. Gjorgjieva, Stability and learning in excitatory synapses by nonlinear inhibitory plasticity, PLOS Computational Biology **18**, 1 (2022).

[25] X. Jiang, S. Shen, C. R. Cadwell, P. Berens, F. Sinz, A. S. Ecker, S. Patel, and A. S. Tolias, Principles of connectivity among morphologically defined cell types in adult neocortex, Science **350**, aac9462 (2015), https://www.science.org/doi/pdf/10.1126/science.aac9462.

[26] A. Litwin-Kumar and B. Doiron, Slow dynamics and high variability in balanced cortical networks with clustered connections, Nature Neuroscience **15**, 1498 (2012).

[27] G. K. Wu, R. Arbuckle, B. hua Liu, H. W. Tao, and L. I. Zhang, Lateral sharpening of cortical frequency tuning by approximately balanced inhibition, Neuron **58**, 132 (2008).

[28] M. L. Sutter and W. C. Loftus, Excitatory and inhibitory intensity tuning in auditory cortex: Evidence for multiple inhibitory mechanisms, Journal of Neurophysiology **90**, 2629 (2003), pMID: 12801894, https://doi.org/10.1152/jn.00722.2002.

[29] G. Liu, Local structural balance and functional interaction of excitatory and inhibitory synapses in hippocampal dendrites, Nature Neuroscience **7**, 373 (2004).

[30] N. Sukenik, O. Vinogradov, E. Weinreb, M. Segal, A. Levina, and E. Moses, Neuronal circuits overcome imbalance in excitation and inhibition by adjusting connection numbers, Proceedings of the National Academy of Sciences **118**, 10.1073/pnas.2018459118 (2021), publisher: National Academy of Sciences Section: Biological Sciences.

[31] S. Zhou and Y. Yu, Synaptic e-i balance underlies efficient neural coding, Frontiers in Neuroscience **12**, 10.3389/fnins.2018.00046 (2018).

[32] T. Vogels and L. Abbott, Gating multiple signals through detailed balance of excitation and inhibition in spiking networks, Nature neuroscience **12**, 483 (2009).

[33] J. Gjorgjieva, C. Clopath, J. Audet, and J.-P. Pfister, A triplet spike-timing–dependent plasticity model generalizes the bienenstock–cooper–munro rule to higher-order spatiotemporal correlations, Proceedings of the National Academy of Sciences **108**, 19383 (2011), https://www.pnas.org/content/108/48/19383.full.pdf.

[34] A. S. Ecker and A. S. Tolias, Is there signal in the noise?, Nature neuroscience **17**, 750 (2014).

[35] D. A. Aponte, G. Handy, A. M. Kline, H. Tsukano, B. Doiron, and H. K. Kato, Recurrent network dynamics shape direction selectivity in primary auditory cortex, Nature Communications **12**, 314 (2021), number: 1 Publisher: Nature Publishing Group.

[36] M. A. Beaumont, J.-M. Cornuet, J.-M. Marin, and C. P. Robert, Adaptive approximate Bayesian computation, Biometrika **96**, 983 (2009).

[37] S. C. Seeman, L. Campagnola, P. A. Davoudian, A. Hoggarth, T. A. Hage, A. Bosma-Moody, C. A. Baker, J. H. Lee, S. Mihalas, C. Teeter, A. L. Ko, J. G. Ojemann, R. P. Gwinn, D. L. Silbergeld, C. Cobbs, J. Phillips, E. Lein, G. Murphy, C. Koch, H. Zeng, and T. Jarsky, Sparse recurrent excitatory connectivity in the microcircuit of the adult mouse and human cortex, eLife **7**, e37349 (2018).

[38] G. A. Wildenberg, M. R. Rosen, J. Lundell, D. Paukner, D. J. Freedman, and N. Kasthuri, Primate neuronal connections are sparse in cortex as compared to mouse, Cell Reports **36**, 109709 (2021).

[39] J. Barral and A. D Reyes, Synaptic scaling rule preserves excitatory–inhibitory balance and salient neuronal network dynamics, Nature Neuroscience **19**, 1690 (2016).

[40] Brunel, Dynamics of sparsely connected networks of excitatory and inhibitory spiking neurons, Journal of Computational Neuroscience **8** (2000).

[41] F. Zenke, E. Agnes, and W. Gerstner, Diverse synaptic plasticity mechanisms orchestrated to form and retrieve memories in spiking neural networks, Nature Communications **6**, 6922 (2015).

[42] E. Giannakakis, F. Hutchings, C. A. Papasavvas, C. E. Han, B. Weber, C. Zhang, and M. Kaiser, Computational modelling of the long-term effects of brain stimulation on the local and global structural connectivity of epileptic patients, PLOS ONE **15**, 1 (2020).

[43] C. Tetzlaff, C. Kolodziejski, I. Markelic, and F. Wörgötter, Time scales of memory, learning, and plasticity, Biological Cybernetics **106**, 10.1007/s00422-012-0529-z (2012).

[44] F. Zenke, W. Gerstner, and S. Ganguli, The temporal paradox of hebbian learning and homeostatic plasticity, Current Opinion in Neurobiology **43**, 166 (2017).

[45] A. Negrón, M. P. Getz, G. Handy, and B. Doiron, The mechanics of correlated variability in segregated cortical excitatory subnetworks, bioRxiv 10.1101/2023.04.25.538323 (2023), https://www.biorxiv.org/content/early/2023/04/27/2023.04.25.538323.full.pdf.

[46] C. Hilgetag and M. Kaiser, Clustered organization of cortical connectivity, Neuroinformatics **2**, 353 (2004).

[47] Y. Yoshimura, J. Dantzker, and E. Callaway, Excitatory cortical neurons form fine-scale functional networks, Nature **433**, 868 (2005).

[48] S. Brown and S. Hestrin, Intracortical circuits of pyramidal neurons reflect their long-range axonal targets, Nature **457**, 1133 (2009).

[49] Z. Ding, P. G. Fahey, S. Papadopoulos, E. Y. Wang, B. Celii, C. Papadopoulos, A. B. Kunin, A. Chang, J. Fu, Z. Ding, S. Patel, K. Ponder, T. Muhammad, J. A. Bae, A. L. Bodor, D. Brittain, J. Buchanan, D. J. Bumbarger, M. A. Castro, E. Cobos, S. Dorkenwald, L. Elabbady, A. Halageri, Z. Jia, C. Jordan, D. Kapner, N. Kemnitz, S. Kinn, K. Lee, K. Li, R. Lu, T. Macrina, G. Mahalingam, E. Mitchell, S. S. Mondal, S. Mu, B. Nehoran, S. Popovych, C. M. Schneider-Mizell, W. Silversmith, M. Takeno, R. Torres, N. L. Turner, W. Wong, J. Wu, W. Yin, S. chieh Yu, E. Froudarakis, F. Sinz, H. S. Seung, F. Collman, N. M. da Costa, R. C. Reid, E. Y. Walker, X. Pitkow, J. Reimer, and A. S. Tolias, Functional connectomics reveals general wiring rule in mouse visual cortex, bioRxiv 10.1101/2023.03.13.531369 (2023), https://www.biorxiv.org/content/early/2023/03/30/2023.03.13.531369.full.pdf.

[50] R. Zeraati, Y.-L. Shi, N. Steinmetz, M. Gieselmann, A. Thiele, T. Moore, A. Levina, and T. Engel, Intrinsic timescales in the visual cortex change with selective attention and reflect spatial connectivity, Nature Communications **14** (2023).

[51] A.-S. Badin, F. Fermani, and S. A. Greenfield, The features and functions of neuronal assemblies: Possible dependency on mechanisms beyond synaptic transmission, Frontiers in Neural Circuits **10**, 10.3389/fncir.2016.00114 (2017).

[52] G. S. Umbach, R. J. Tan, J. Jacobs, B. E. Pfeiffer, and B. C. Lega, Flexibility of functional neuronal assemblies supports human memory, Nature Communications **13** (2021).

[53] S. Hofer, H. Ko, B. Pichler, J. Vogelstein, H. Ros, H. Zeng, E. Lein, N. Lesica, and T. Mrsic-Flogel, Differential connectivity and response dynamics of excitatory and inhibitory neurons in visual cortex, Nature neuroscience **14**, 1045 (2011).

[54] R. B. Levy and A. D. Reyes, Spatial profile of excitatory and inhibitory synaptic connectivity in mouse primary auditory cortex, Journal of Neuroscience **32**, 5609 (2012), https://www.jneurosci.org/content/32/16/5609.full.pdf.

[55] G. Mongillo, S. Rumpel, and Y. Loewenstein, Inhibitory connectivity defines the realm of excitatory plasticity, Nature neuroscience **21**, 1463 (2018).

[56] F. Lagzi, M. C. Bustos, A.-M. Oswald, and B. Doiron, Assembly formation is stabilized by parvalbumin neurons and accelerated by somatostatin neurons, bioRxiv 10.1101/2021.09.06.459211 (2021), https://www.biorxiv.org/content/early/2021/09/07/2021.09.06.459211.full.pdf.

[57] K. Cranmer, J. Brehmer, and G. Louppe, The frontier of simulation-based inference, Proceedings of the National Academy of Sciences , 201912789 (2020).

[58] J.-M. Lueckmann, J. Boelts, D. Greenberg, P. Goncalves, and J. Macke, Benchmarking simulation-based inference, in *International Conference on Artificial Intelligence and Statistics* (PMLR, 2021) pp. 343–351.

[59] P. J. Gonçalves, J.-M. Lueckmann, M. Deistler, M. Nonnenmacher, K. Öcal, G. Bassetto, C. Chintaluri, W. F. Podlaski, S. A. Haddad, T. P. Vogels, D. S. Greenberg, and J. H. Macke, Training deep neural density estimators to identify mechanistic models of neural dynamics, eLife **9**, e56261 (2020), publisher: eLife Sciences Publications, Ltd.

[60] G. Bellec, F. Scherr, A. Subramoney, E. Hajek, D. Salaj, R. Legenstein, and W. Maass, A solution to the learning dilemma for recurrent networks of spiking neurons, Nature Communications **11** (2020).

[61] F. Zenke and T. P. Vogels, The Remarkable Robustness of Surrogate Gradient Learning for Instilling Complex Function in Spiking Neural Networks, Neural Computation **33**, 899 (2021), https://direct.mit.edu/neco/article-pdf/33/4/899/1902294/neco_a_01367.pdf.

[62] N. Caporale and Y. Dan, Spike timing–dependent plasticity: A hebbian learning rule, Annual review of neuroscience **31**, 25 (2008).

[63] One could argue that external noise should be interpreted as Stratonovich and internal as Itô. Since both noises are additive, this difference is not so relevant and we treat both noises as Itô for simplicity.

[64] C. Gardiner, *Stochastic Methods: A Handbook for the Natural and Social Sciences*, Springer Series in Synergetics (Springer, 2009).

.

Appendix 1: The effects of inhomogeneous connectivity are independent of the plasticity protocols' details

We examined whether our results are dependent on the particular plasticity protocol we used [21], and we verified that they hold for alternative plasticity mechanisms. At first, we examine our result's robustness with respect to the form of the excitatory and inhibitory learning rules used, while maintaining the same competitive normalization protocol [21]. We find that replacing the triplet rule [33] with a classic spike pair Hebbian rule [62] leads to no discernible effect in the quality of the tuning. Furthermore, we examine a variety of different LTD and LTP amplitudes in the excitatory plasticity as well as several target rates ρ_0 for the inhibitory plasticity without observing any noticeable changes on our main findings
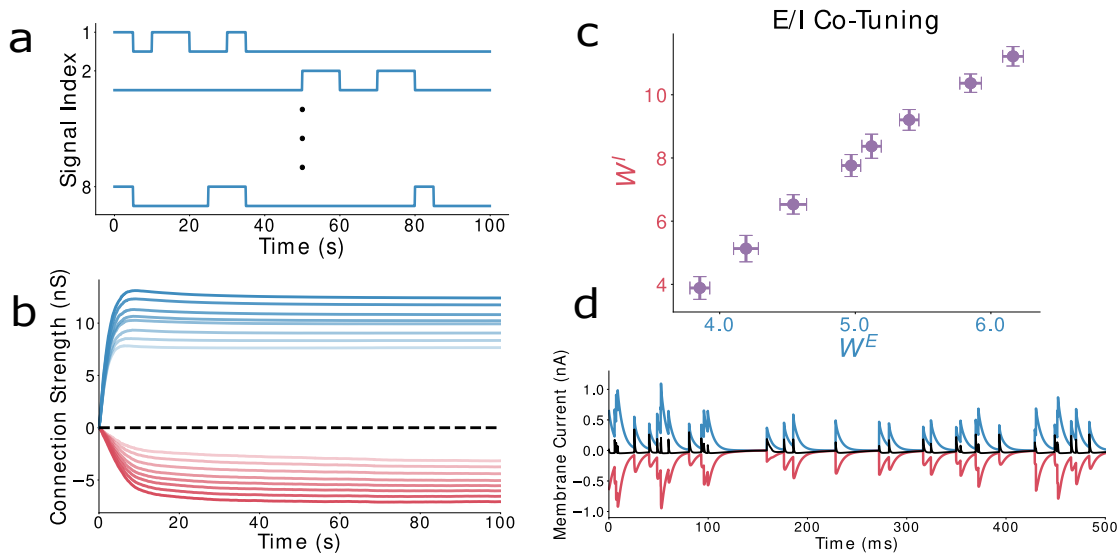

FIG. 5. **Alternative plasticity protocol. a.** For diversity to emerge, there needs to be a mechanism that enforces inhomogeneity in the presynaptic firing rates, such as pulses of input. **b.** Given such a mechanism, the weights converge rapidly, in a state of near-perfect E/I co-tuning (**c**), leading to very tight balance of incoming E/I currents (**d**).

Moreover, we studied both the triplet [33] and pair Hebbian rules [62] combined with a subtractive normalization mechanism that has been previously used in plasticity studies [11] :

$$\Delta W_k^E = \frac{\sum_{i=1}^{N_A} W_{ik}^E - W^{target}}{N_E} \qquad (11)$$

In 2016 [20] it was demonstrated that subtractive normalization only on the excitatory connections will lead to all the weights converging on the same point due to the inhibitory plasticity creating a moving threshold. In order to prevent this collapse of the receptive field, enforced inhomogeneity on the firing rates of different groups is needed. We solved this problem by giving the network's input as pulses of 500 mS, enforcing inhomogeneous firing rates which result in the emergence of diverse and balanced feedforward connectivity.

We verified that the co-tuning achieved in this setting, similar to the mechanism presented in the main text, suffers from the introduction of noise and recurrent connectivity. Furthermore, the assembling principles that we derived for the original network, seem to have a similarly beneficial effect on this setting, restoring the original covariance structure of the network's activity and leading to detailed co-tuning between the E and I feedforward connections.

Appendix 2: Convergence of weights to an eigenvector of the covariance matrix under plasticity

We verify that our model agrees with the analytics of previous studies [7, 20, 21] that the convergence point of the weights is an eigenvector of the modified covariance matrix:

$$\overline{C} = \left\langle \begin{pmatrix} EE^T & -IE^T \\ EI^T & -II^T \end{pmatrix} \right\rangle \tag{21}$$

where E, I are the activities of the excitatory and inhibitory populations respectively.
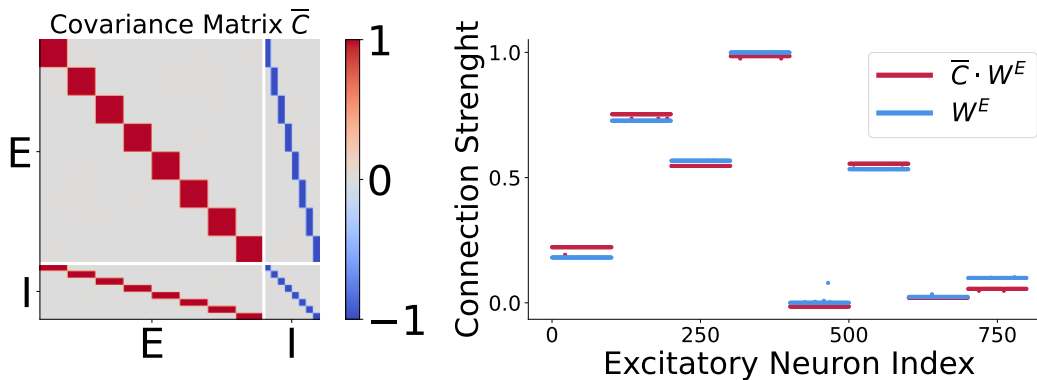

FIG. 6. **Weights converge to an eigenvector of the covariance matrix.** A: The estimated covariance matrix for a feedforward network. B. We verify that the convergence point of the weights is an eigenvector of the covariance matrix.

Specifically, we multiply the converged weight vector with a numerical calculation of the covariance (estimated via binning of the spike trains with a bin size of 1 mS) and verify that the resulting product is approximately equal to a multiple of the original weight matrix.

Appendix 3: Perturbation of the optimal assembly strengths leads to diverse effects on the network's activity

To investigate the relative importance of the different connection types, we perturb various assemblies away from the optimal solutions inferred with ABC and check the resulting changes on the network activity as well as how fast the balance and diversity deteriorate.

We find that $I \to E$ assemblies have a strong impact on the resulting network dynamics and consequently the statistics that determine the emergence of co-tuning Fig. 7e. Thus, when $I \to E$ assemblies are too strong, the network exhibits synchronous behavior that does not allow the discrimination between neuron groups and consequently the emergence of co-tuned connectivity. In contrast, when $I \to E$ assemblies are too weak, one group of neurons is constantly active. This eventually leads to perfect discrimination of only a single input.

$E \to E$ assemblies also have a strong effect on the resulting learned connectivity. When they are reduced, the weights diversity rapidly reduces, while the balance metric first decreases and then restores. This behavior is related to two different bifurcations in the population dynamics. First, synchronous full-network bursts emerge on top of the stimulus-induced firing Fig. 7a. Then, as $E \to E$ are reduced further, the network enters an asynchronous irregular state Fig. 7a.

Perturbations of $I \to I$ and $E \to I$ assemblies have weaker effect on the balance and weight diversity. Specifically, when $I \to I$ assemblies are weakened the network displays synchronous bursts on top of the stimulus-driven activity that only minimally reduce the balance and weights diversity Fig. 7d. When $E \to I$ assemblies are reduced, the weight diversity slowly decreases, due to a decrease in the diversity of inhibitory weights. Thus, activity of inhibitory population becomes more discoordinated Fig. 7c. On the other hand, network with uniform $E \to I$ connections (i.e., without $E \to I$ assemblies), show a dramatic reduction in the balance metric because of very strong activation of a single neuron group accompanied by simultaneous activity of all inhibitory neurons Fig. 7c.
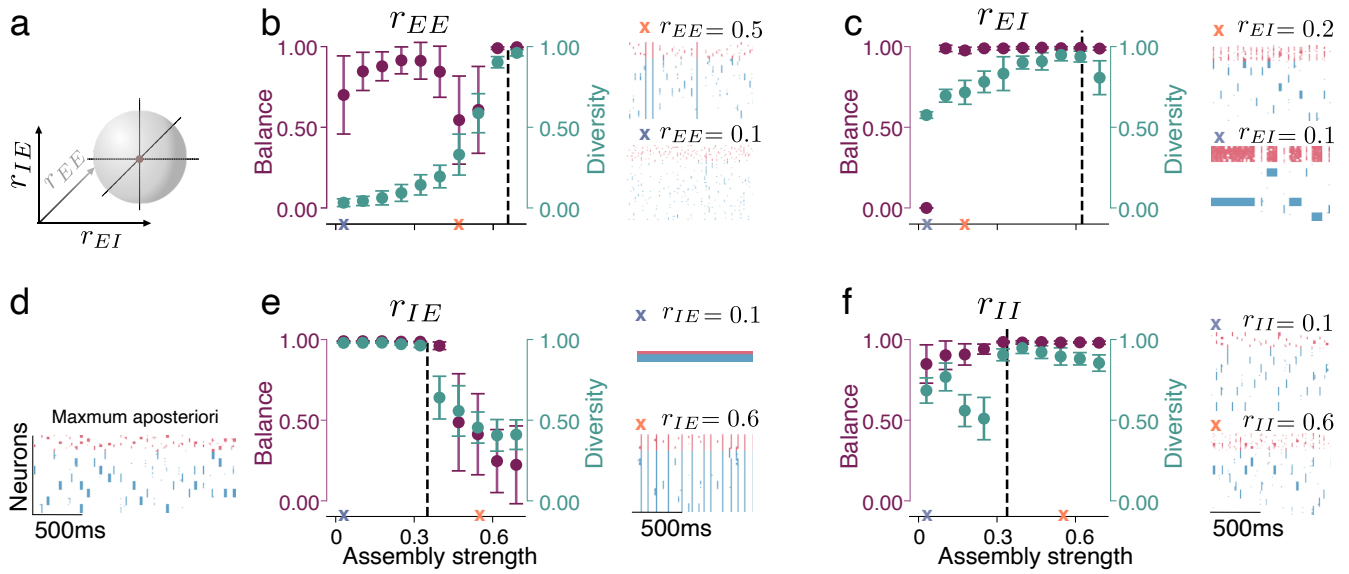
FIG. 7. **Changes of the various assemblies strengths differently affect balance and diversity. a.** We sequentially vary the value of each assembly strength, while keeping the rest of the parameters fixed at the maximum a posteriori (MAP) solution (**d**). **b.** A decrease in the $E \to E$ assembly strength (R_{EE}) introduces synchronous burst-like events that jeopardize co-tuning and weight diversity. Further reduction of the $E \to E$ assembly strength results in sparse, asynchronous spiking which significantly reduces tuning quality. **c.** Reduction of $E \to I$ assembly strength first leads to synchronous inhibitory firing across groups and further reduction leads to persistent activity of the whole inhibitory population combined with bursts of excitatory activity that prevent the development of diversity. **e.** Decreasing the $I \to E$ assembly strength leads to persistent activation of a single group of neurons (which affects the tuning only marginally). While the increase of the $I \to E$ assembly strength leads to oscillatory behavior of the whole network. **f.** Weakening the $I \to I$ assemblies decreases the weight diversity by introducing occasional synchronous bursts in the network, while strengthening them leads to asynchronous inhibitory activity.

Appendix 4: Reduced model calculations

1. Derivation of the equations

In this Appendix, we start from main text Eqs. 14,

$$\dot{x}_i = ax_i + by_i + \frac{1}{M-1}\sum_{j\neq i}\left(W^{EE}x_j + W^{EI}y_j\right) + \sigma_{\text{int}}\xi_i^x(t) + \sigma_{\text{ext}}\eta_i(t) + \eta_0, \tag{41a}$$

$$\dot{y}_i = cx_i + dy_i + \frac{1}{M-1}\sum_{j\neq i}\left(W^{IE}x_j + W^{II}y_j\right) + \sigma_{\text{int}}\xi_i^y(t) + \sigma_{\text{ext}}\eta_i(t) + \eta_0. \tag{41b}$$

where we consider M groups composed by excitatory $x_i(t)$ and inhibitory $y_i(t)$ populations $(i = 1, \ldots, n)$ coupled linearly (see also Methods). Internal noise of each population is represented by $\xi_i^x(t)$ and $\xi_i^y(t)$ for excitatory and inhibitory populations, respectively. On the other hand, external noise $\eta_i(t)$ is shared among both populations. All the noises have zero mean and correlations

$$\left\langle \xi_i^c \xi_j^{c'} \right\rangle = \delta_{cc'}\delta_{ij}\delta(t - t'), \tag{42a}$$

$$\langle \xi_i^c(t)\eta_j(t')\rangle = 0 \quad \forall i, j, t, t', \tag{42b}$$

$$\langle \eta_i(t)\eta_j(t')\rangle = \delta_{ij}\delta(t - t'). \tag{42c}$$

We will derive closed expressions for the correlation coefficients. We would like to remark that $\langle \cdot \rangle$ means an ensemble average over noise realizations. All stochastic equations are to be interpreted in the Itô convention[63].

First of all, we redefine the noise terms, which will prove convenient later to simplify the algebra. For this reason, we define

$$\xi_i^1(t) = \sigma_{\text{int}}\xi_i^x(t) + \sigma_{\text{ext}}\eta_i(t), \tag{43a}$$

$$\xi_i^2(t) = \sigma_{\text{int}}\xi_i^y(t) + \sigma_{\text{ext}}\eta_i(t), \tag{43b}$$

which are Gaussian white noises with zero mean and correlation matrix

$$\left\langle \xi_i^1(t)\,\xi_j^1(t')\right\rangle = \left\langle \xi_i^2(t)\,\xi_j^2(t')\right\rangle = \delta_{ij}\delta(t-t')\left(\sigma_{int}^2 + \sigma_{ext}^2\right), \tag{44a}$$

$$\left\langle \xi_i^1(t)\,\xi_j^2(t')\right\rangle = \delta_{ij}\delta(t-t')\,\sigma_{ext}^2. \tag{44b}$$

To start with, one can obtain the average values for the stationary rates by applying averages to both sides of equations (41) and imposing the stationary state condition, $\langle \dot{x}_i\rangle = \langle \dot{y}_i\rangle = 0$. Once this is done, it is immediate to solve the resulting linear system and check that $\langle x_i^*\rangle, \langle y_i^*\rangle \propto \eta_0$, where the star (*) indicates that these values correspond to the stationary state. Hence, making $\eta_0 = 0$ the mean values vanish. One can demonstrate that correlations do not depend on η_0, and hence we can make $\eta_0 = 0$ without loss of generality. Conceptually, this means just shifting up or down the baseline of fluctuations of the firing rate, which does not affect the fluctuations themselves.

In order to compute correlations, we need to evaluate the second-order moments between different populations, as $\langle x_i y_j\rangle$ or $\langle x_i^2\rangle$. A possible way of doing this is starting from the analytical solution of the multidimensional Orstein-Uhlenbeck process [64]. However, this approach will yield a linear system with $N(N+1)/2$ variables to solve for, which are all the elements of the (symmetric) correlation matrix. But all the groups are identical (or *indistinguishable*), so we expect correlations not to depend on the particular population chosen. Therefore, all the equations will be reduced to just 6 covariances: $\langle x_i x_j\rangle$, $\langle x_i y_j\rangle$, $\langle y_i y_j\rangle$, $\langle x_i^2\rangle$, $\langle x_i y_i\rangle$ and $\langle y_i^2\rangle$.

In this context, it is conceptually simpler to obtain equations for the evolution of the second moments, and then evaluate them in the stationary state. We report here in detail the computation of two of these moments as an example, giving just the final answer for the other four, which is performed in an analogous way.

First, we define $X_{ij} = x_i x_j$, and then look for the time evolution of X_{ij}, i.e., $\dot{X}_{ij}$. Notice that this a non-linear change of variables, and thus Itô's lemma is required. The lemma tells us that if we have a change of variables $z = z(x)$ then one has to include the second-order terms in the expansion,

$$dz = \underbrace{\sum_{i=1}^N \partial_{x_i} z\, dx_i}_{\text{Chain rule}} + \underbrace{\frac{1}{2}\sum_{i=1}^N \partial_{x_i}\partial_{x_j} z\, dx_i dx_j}_{\text{Itô's lemma}}. \tag{45}$$

The terms dx_i can be obtained as $\dot{x}_i dt$. It is important to remark that in this procedure noise terms are rewritten as the differential of the Wiener processes, i.e., $\eta_i(t)dt = dW_i$. After applying the Itô lemma above, only terms up to order dt should be taken into account. Notice that $dW_i(t) \propto \sqrt{dt}$ [64]. Finally, one just divides again by dt to recover the stochastic differential equation and applies the ensemble average.

For X_{ij}, this reads as

$$\frac{d\langle x_i x_j\rangle}{dt} = \langle \dot{x}_i x_j\rangle + \langle x_i \dot{x}_j\rangle + \frac{1}{2}\langle \dot{x}_i \dot{x}_j\rangle =$$

$$a\langle x_i x_j\rangle + b\langle y_i x_j\rangle + \frac{W^{EE}}{M-1}\sum_{k\neq i}\langle x_k x_j\rangle + \frac{W^{EI}}{M-1}\sum_{k\neq i}\langle y_k x_j\rangle +$$

$$+ a\langle x_i x_j\rangle + b\langle x_i y_j\rangle + \frac{W^{EE}}{M-1}\sum_{k\neq j}\langle x_i x_k\rangle + \frac{W^{EI}}{M-1}\sum_{k\neq j}\langle x_i y_k\rangle +$$

$$\langle \xi_i^1 x_j\rangle + \langle x_i \xi_j^1\rangle + \langle \xi_i^1 \xi_j^1\rangle + \mathcal{O}\left(dt^2\right), \tag{46}$$

where all the averages between the noise and the variable yield 0, due to Itô's prescription. The next step is to simplify the sums involving correlations. As it was discussed above, since clusters are indistinguishable all the terms are exactly the same. However, the dummy index k will take also the value of the fixed index, $k = j$, and this has to be taken into account separately since the in-group is different to the between-group one. Then,

$$\sum_{k\neq i}\langle x_k x_j\rangle = (M-2)\langle x_i x_j\rangle + \langle x_i^2\rangle, \tag{47}$$

allowing us to simplify the equation. At this step we simplify the notation by letting $X_{ij} = \langle x_i x_j \rangle$, $Z_{ij} = \langle x_i y_j \rangle$, $Y_i = \langle y_i^2 \rangle$, etc., leading to

$$\frac{1}{2}\dot{X}_{ij} = \left(a + \frac{M-2}{M-1}W^{EE}\right)X_{ij} + \left(b + \frac{M-2}{M-1}W^{EI}\right)Z_{ij} + \frac{1}{M-1}\left[W^{EE}X_i + W^{EI}Z_i\right]. \tag{48}$$

The same procedure can be repeated for all the other correlations, such as

$$\frac{d\langle y_i^2 \rangle}{dt} = \langle 2y_i\dot{y}_i \rangle + \frac{1}{2}\langle 2\dot{y}_i^2 \rangle =$$

$$2c\langle x_i y_i \rangle + 2d\langle y_i^2 \rangle + \frac{2W^{IE}}{M-1}\sum_{k\neq i}\langle y_i x_k \rangle + \frac{2W^{II}}{M-1}\sum_{k\neq i}\langle y_i y_k \rangle + 2\langle y_i\xi_i^2 \rangle + \langle \xi_i^2\xi_i^2 \rangle =$$

$$2c\langle Z_i \rangle + 2d\langle Y_i \rangle + 2W^{IE}\langle Z_{ij} \rangle + 2W^{II}\langle Y_{ij} \rangle + \sigma_{\text{int}}^2 + \sigma_{\text{ext}}^2, \tag{49}$$

where now the correlation between noises yields a non-vanishing value. This operation is repeated with all the remaining terms, in order to find a linear system of differential equations with 6 variables and 6 equations,

$$\frac{1}{2}\dot{X}_i = aX_i + bZ_i + \left[W^{EE}X_{ij} + W^{EI}Z_{ij}\right] + \frac{1}{2}\left(\sigma_{\text{int}}^2 + \sigma_{\text{ext}}^2\right), \tag{410a}$$

$$\frac{1}{2}\dot{Y}_i = cZ_i + dY_i + \left[W^{IE}Z_{ij} + W^{II}Y_{ij}\right] + \frac{1}{2}\left(\sigma_{\text{int}}^2 + \sigma_{\text{ext}}^2\right), \tag{410b}$$

$$\dot{Z}_i = cX_i + (a+d)Z_i + bY_i + \left[W^{IE}X_{ij} + \left(W^{EE} + W^{II}\right)Z_{ij} + W^{EI}Y_{ij}\right] + \sigma_{\text{ext}}^2, \tag{410c}$$

$$\frac{1}{2}\dot{X}_{ij} = \left(a + \frac{M-2}{M-1}W^{EE}\right)X_{ij} + \left(b + \frac{M-2}{M-1}W^{EI}\right)Z_{ij} + \frac{1}{M-1}\left[W^{EE}X_i + W^{EI}Z_i\right], \tag{410d}$$

$$\frac{1}{2}\dot{Y}_{ij} = \left(d + \frac{M-2}{M-1}W^{II}\right)Y_{ij} + \left(c + \frac{M-2}{M-1}W^{IE}\right)Z_{ij} + \frac{1}{M-1}\left[W^{II}Y_i + W^{IE}Z_i\right], \tag{410e}$$

$$\dot{Z}_{ij} = \left(c + \frac{M-2}{M-1}W^{IE}\right)X_{ij} + \left(b + \frac{M-2}{M-1}W^{EI}\right)Y_{ij} + \left(a + d + \frac{M-2}{M-1}\left(W^{EE} + W^{II}\right)\right)Z_{ij} + \tag{410f}$$

$$+ \frac{1}{M-1}\left[W^{IE}X_i + W^{EI}Y_i + \left(W^{EE} + W^{II}\right)Z_i\right]. \tag{410g}$$

This system can be solved in the stationary limit when all the derivatives of the left-hand side are zero. From these, one is able to obtain the Pearson correlation coefficients. Correlation with itself is always unity, thus there are only four coefficients remaining: the correlation between excitation and inhibition inside a group $C_{EI}^{\text{int}} = Z_i^*/\sqrt{X_i^* Y_i^*}$, and all three between-group correlations, $C_{EE}^{\text{ext}} = X_{ij}^*/X_i^*$, $C_{II}^{\text{ext}} = Y_{ij}^*/Y_i^*$, and $C_{EI}^{\text{ext}} = Z_{ij}^*/\sqrt{X_i^* Y_i^*}$.

2. Solutions for the homogeneous network

In some special cases, it is possible to give a simple solution in closed form for the correlation coefficients. One example is the homogeneous network: when all weights are identical, and an intrinsic decay is added to both the excitatory and inhibitory populations (i.e., with $c = W^{EE} = W^{IE} = +W$, $b = W^{IE} = W^{II} = -W$ and $a = W-1$, $d = -W-1$) the solution reads

$$C_{EI}^{\text{int}} = \frac{r^2(M-1)^2 + W^2(1-r)^2 M}{\sqrt{M^2(1-r)^4 W^4 + (M-1)(1-r)^2W^2\left[M(2-4(1-r)r)-(1-r)^2\right] + (M-1)^4\left[2(r-1)r+1\right]^2}}, \tag{411a}$$

$$C_{EI}^{\text{ext}} = \frac{W^2(1-r)^2 M}{\sqrt{M^2(1-r)^4 W^4 + (M-1)(1-r)^2W^2\left(M(4(r-1)r+2)-(r-1)^2\right) + (M-1)^4(2(r-1)r+1)^2}}, \tag{411b}$$

$$C_{EE}^{\text{ext}} = \frac{(1-r)^2W\left((W+1)M-1\right)}{M(1-r)^2W^2 + (M-1)(1-r)^2W + (1-M)^2\left[1-2(1-r)r\right]}, \tag{411c}$$

$$C_{II}^{\text{ext}} = \frac{(1-r)^2W\left((W-1)M+1\right)}{M(1-r)^2W^2 - (M-1)(1-r)^2W + (1-M)^2\left[1-2(1-r)r\right]}, \tag{411d}$$

where we defined r as the signal-to-noise ratio, $\sigma_{\text{int}} = r\sigma$, $\sigma_{\text{ext}} = (1 - r)\sigma$. This analytical solution has some interesting features. First, notice it does not depend on the total amount of noise σ that the system receives, but only on the ratio between external and internal noise. Second, if $W \to \infty$ all correlations go to 1, making the diversity between groups vanish. Expanding in series around $\epsilon = 1/W = 0$, one can see that all coefficients are $C = 1 - \mathcal{O}(1/W^2)$ for large coupling.
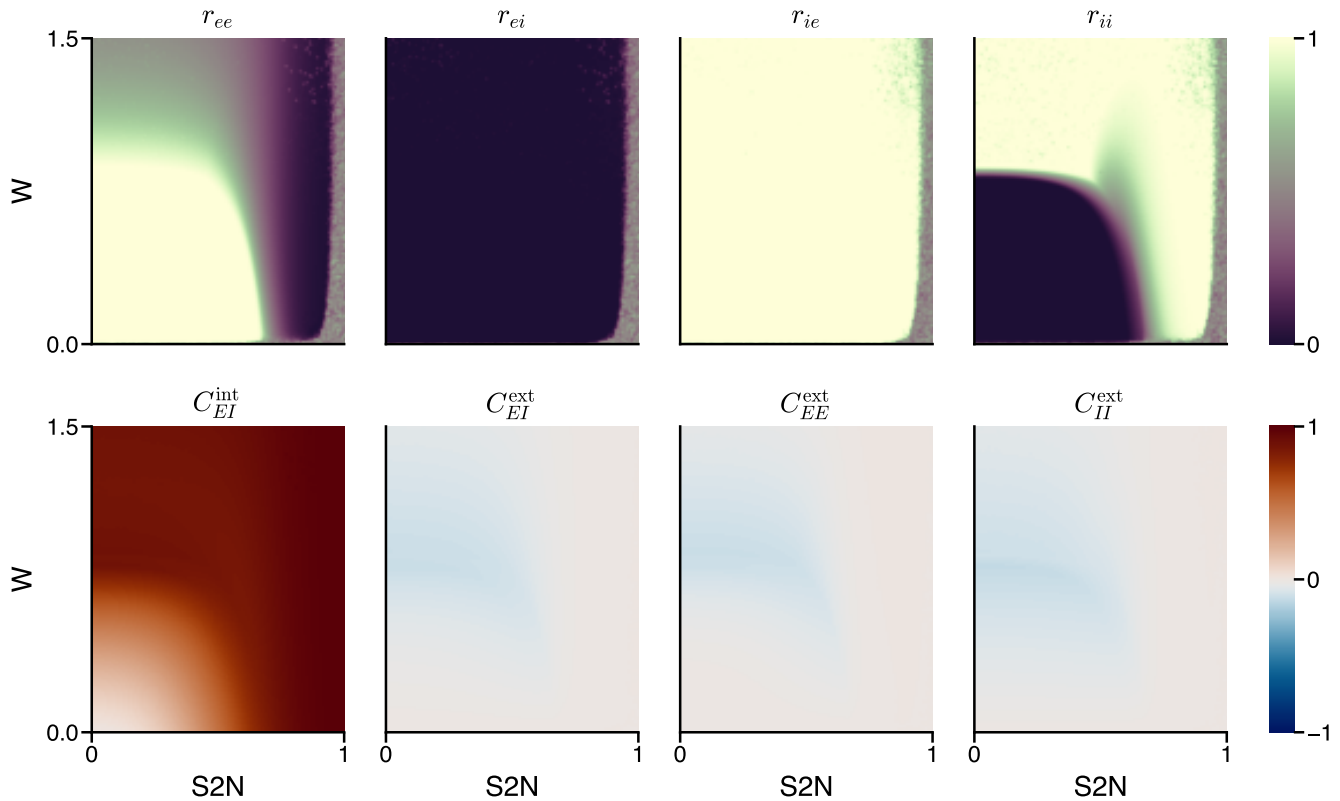

FIG. 8. Optimical clustering for the analytical results. The selected values of the clustering lead to large decorrelations between different groups. Large correlations in-group can be achieved for a large set of recurrence and external noise. In this case, highly clustered excitation and homogeneous inhibition is recovered.

It is also possible to study the limiting values of the noise. $r = 1$ makes all the between-group correlations equal to zero, while coupling determines the in-group value. On the other hand, when $r \ll 1$, one gets

$$C_{EI}^{\text{int}} \simeq C_{EI}^{\text{ext}} \simeq \frac{MW^2}{(M-1)^2} + \mathcal{O}(r^2), \tag{412a}$$

$$C_{EE}^{\text{ext}} \simeq -C_{II}^{\text{ext}} \simeq \frac{W}{M-1} + \mathcal{O}(r^2). \tag{412b}$$

meaning that the external correlations grow linearly with the coupling, but quadratically with the signal-to-noise ratio: a small increase in coupling needs to be followed by a larger increase in signal intensity in order to recover the previous tuning. As a result, the coupling has a larger impact on tuning than the signal-to-noise ratio, an effect that can be measured in the full spiking network.

Finally, we see that between-group correlations also tend to zero as the limit $M \to +\infty$ is taken, since in that case, the input that a module receives from all others becomes just white noise. A finite number of clusters (or finite connectivity among them) is thus required for tuning.

Appendix 5: Clustering optimisation

Optimization of the clustering for the fully-connected network can be done by minimizing a loss function which depends on the correlations. A simple possibility is to employ minimum squares,

$$\mathcal{L}^{an}[C;p] = \left(1 - C_{EI}^{\text{int}}\right)^2 + \left(C_{EE}^{\text{ext}}\right)^2 + \left(C_{EI}^{\text{ext}}\right)^2 + \left(C_{II}^{\text{ext}}\right)^2. \tag{51}$$

The solution and associated optimal correlations are shown in 8. There are several key remarks following from this figure:

1. Even for very large clustering and extremely low signal-to-noise ratio, the clustering is able to provide an in-group correlation close to unity combined with low between-group correlations, thus ensuring co-tuning.

2. Inhibition to excitation never clusters. Inhibitory neurons act over excitatory individuals regardless of their cluster.

3. Excitatory connections are clustered. In particular, excitatory connections always project to inhibitory neurons in their own cluster, but not to other ones. Excitatory-to-excitatory connectivity is also strongly clustered, except for large coupling.

4. Inhibition controls excitation for large W. If one keeps highly clustered excitation and increases the coupling, the dynamics of single modules become unstable at a critical value $W_c(r)$. However, the network can remain stable if the excitatory clustering is reduced and the amount of inhibition in the group increases, which can be accomplished by increasing r_{II}.

5. When the signal-to-noise ratio is close to one, clustering becomes mostly irrelevant, since the system is driven by the external input which allows co-tuning easily.

Notice that the optimization algorithm automatically finds solutions where the equations are well-defined –i.e., where the system reaches a stationary state– thus selecting to increase the inhibitory clustering when W goes over the instability threshold.

Therefore, the analytical approach is able to find a good candidate for optimal clustering depending on the network dynamics. Although it cannot be directly applied to the spiking network, which is able to display richer dynamics, tells us that as a rule of thumb excitatory clustering should be as high as possible while avoiding crossing an instability threshold. If this happens, inhibition needs to be increased.

Appendix 6: Tables of parameters

We mostly used the neuron model parameters from the original inhibitory STDP paper [7]

Network Model		
Symbol	Description	Value
N	Number of neurons	1000
N_E	Number of E neurons	800
N_I	Number of I neurons	200
M	Number of input groups	8
g_{leak}	Leak conductance	10 nS
V_{rest}	Resting potential	-60 mV
V_{reset}	Reset potential	-60 mV
V_{th}	Spiking threshold	-50 mV
V_E	Excitatory reversal potential	0 mV
V_I	Inhibitory reversal potential	-80 mV
C_m	Membrane capacitance	200 pF
τ_{ref}	Absolute refractory period	5 ms
τ_E	Decay time constant of E conductance	5 ms
τ_I	Decay time constant of I conductance	10 ms
$\overline{g_E}$	E weight scaling constant	1.4 nS
$\overline{g_I}$	I weight scaling constant	3.5 nS

Plasticity Rules		
Symbol	Description	Value
τ_1^{estdp}	Slow eSTDP timescale	50 ms
τ_2^{estdp}	Fast eSTDP timescale	10 ms
η_E	eSTDP learning rate	0.0025
A_{LTP}	Long term potentiation amplitude	1.0
A_{LTD}	Long term depression amplitude	0.1
τ^{istdp}	iSTDP timescale	10 ms
η_I	iSTDP learning rate	0.01
ρ_0	iSTDP target rate	3 Hz
η_N	Normalization learning rate	0.003
W_{target}^E	Excitatory normalization target	5.0
W_{target}^I	Inhibitory normalization target	5.0

ABC Optimization		
Symbol	Description	Value
α	weight of in-group correlation	0.1
β	weight of between-group correlations	0.3